MeV X-Ray Generation with a Femtosecond Laser

J. D. Kmetec, C. L. Gordon, III, J. J. Macklin, B. E. Lemoff, G. S. Brown,[a] and S. E. Harris
E. L. Ginzton Laboratory, Stanford University, Stanford, California 94305
(Received 17 December 1991)

A 0.5-TW, 120-fs Ti:sapphire laser, when focused to greater than 10^{18} W/cm^2 onto a solid target, creates a plasma which emits radiation that extends beyond 1 MeV. The x-ray yield increases as the $\frac{3}{2}$ power of the incident laser energy, reaching 0.3% energy conversion to radiation above 20 keV at 40 mJ of laser energy on target. An x-ray spectral distribution of $1/E$ fits the data for most of the radiation, falling faster at higher photon energies.

PACS numbers: 52.25.Nr, 42.65.Re, 52.50.Jm

This Letter reports the generation of hard-x-ray radiation (20 keV to 1 MeV) by focusing a femtosecond laser onto a heavy metal at an intensity greater than 10^{18} W/cm^2. We use a recently developed Ti:sapphire laser system which produces a 60-mJ, 120-fs pulse at 807 nm, at a pulse repetition rate of 5 Hz [1]. We observe a maximum conversion efficiency of incident laser energy to x-ray energy of 0.3% (assuming an isotropic emission), which increases as the $\frac{3}{2}$ power of the incident laser energy. Our spectral data are well fitted by a $1/E$ distribution (x-ray yield per bandwidth) for most of the detected radiation (20 to $\sim$200 keV), while the spectrum falls faster than $1/E$ at higher photon energies. We estimate about 10^6 photons above 1 MeV are generated with each laser pulse.

There have recently been several experiments and studies concerned with the generation of short pulses of x rays with high power femtosecond lasers [2–6]. In these experiments the laser energy on target ranges from 2 to 250 mJ, and the highest reported x-ray energies are several keV. In contrast, we report very-hard-x-ray emission, extending 2 or 3 orders of magnitude higher in photon energy, using only 40 mJ of laser energy. It is likely that the radiation arises from the bremsstrahlung emission of very energetic electrons traversing the solid target. It is not clear what laser-plasma interaction mechanism produces such hot electrons on this femtosecond time scale. Hard-x-ray emission from laser-produced plasmas has been observed previously only with very large kilojoule-level laser systems, operating in the nanosecond regime [7].

To generate the x rays, we focus the laser pulse with a 5-cm focal length, diamond turned, off-axis paraboloid. At low laser power, observation of the focal region with a microscope objective and a charge-coupled-device camera indicates that 60% of the energy falls within a 3-μm-diam spot. With 40 mJ of incident energy, we anticipate the focal intensity to be near 3 EW/cm^2 (1 EW $=10^{18}$ W). The focused pulse is incident on a solid tantalum target (1 mm thick) at 30° from the normal, with p polarization. The round target is rotated and translated to expose a fresh surface for each shot of the laser. Surface preparation consists of only a rough polish and no experiments were conducted to determine the effect of surface preparation. A background gas of 20 Torr of air helps prevent the sputtering of target material onto the optics in the chamber. The x-ray yield was not measurably affected until about 40 Torr of air was introduced. Additionally, a 2-μm nitrocellulose pellicle is sometimes included to protect the parabolic surface.

A low intensity background pulse, which arises from amplified spontaneous emission in the amplifiers, precedes the main pulse in time. The prepulse is approximately 6 orders of magnitude less intense, and occurs for about 2 nsec before the main pulse. This is roughly 1 mJ of energy, and is sufficient to preionize the target. As the incident laser energy on target is varied, the amount of energy in the prepulse varies accordingly, such that the peak intensity to prepulse intensity ratio is always about 10^6. The prepulse appears to be necessary for efficient x-ray production, although the x rays do not appear to be sensitive to the precise prepulse condition.

As shown in Fig. 1, the x rays exit from the target chamber through a 3.2-mm-thick acrylic window, located 18 cm from the plasma. This window is 60° from the target normal (opposite the laser beam), and in the same horizontal plane of the laser beam. An aperture is used near the source to collimate the x-ray beam. This aper-

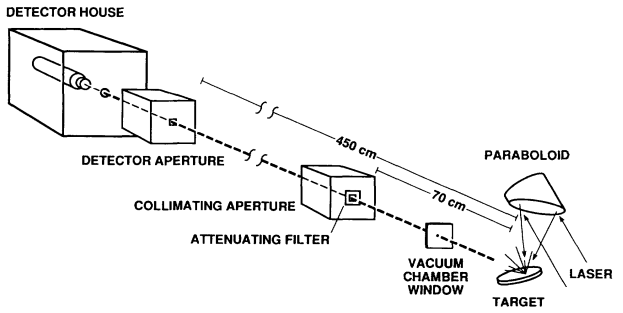

FIG. 1. Geometry of the x-ray generation and detection system. The target is rotated and translated for every shot, and the plasma occurs in a chamber containing 20 Torr of air. The tunnel apertures are constructed from 20-cm lead bricks, and the detector is completely enclosed in a 5-cm-thick wall lead brick house.

ture is a 3.2-mm hole in a 20-cm-thick lead wall, 70 cm from the plasma. The detector aperture is 450 cm from the plasma, and is formed by a hole in a 20-cm-thick block of lead. Typically, this hole was 0.025 cm^2, hence collecting a solid angle of 1.2×10^{-7} sr from the source. The 20-cm thickness is required for sufficient opacity. The detector is a 25.4-mm NaI(Tl) crystal (Bicron 1M1) with a phototube and field-effect-transistor preamplifier. It is enclosed in a 1.6-mm wall thickness aluminum tube and a 3.2-mm wall thickness brass outer tube. This assembly is fully enclosed in a lead brick house, with a minimum wall thickness of 5 cm. The aluminum and brass tubes help eliminate interfering lead fluorescence. A 6.3-mm hole in the lead, centered on the NaI crystal, forms the entrance aperture for the x rays.

A second NaI(Tl) detector, not shown in Fig. 1, is used to monitor overall x-ray yield for each shot, for use as a diagnostic. It is shielded with lead, except for a 6.3-mm entrance port for the x rays. It uses a 3.2-mm-thick piece of aluminum as a filter to remove x rays below 30 keV, and the 1-mm NaI crystal is relatively insensitive to x rays above 100 keV. Most of the x rays fall within this pass band. It is located 80 cm from the plasma, viewing nearly the same angle as the other detector. This detector is used to insure optimal focusing (distance between the paraboloid and the target), although some vivid visible indications are present. The scattered light from the plasma qualitatively correlates with the x-ray production. Under poor focusing, the visible scattered light is mostly blue, measured to be the second harmonic of the incident laser. Improved focusing creates green, corresponding to the $\frac{3}{2}$ harmonic of the laser. Best focusing causes the scattered light to be bright white. The hard x rays become detectable approximately when the green scattered light is visible, and continue to increase as the focusing improves. 10 mJ of incident laser energy under optimal focusing yields a strong green scatter, while 40 mJ at optimal focusing is bright white.

The x-ray spectrum is determined by two complementary methods. In the 20–300-keV region, the spectrum is determined by measuring the total energy deposited in the detector in the presence of different attenuating foils; the spectral discriminator is the functional dependence of attenuation versus frequency of the different foils. For photon energies above about 300 keV, the attenuators lose their energy selectivity, and we use single-photon pulse-height analysis to determine a spectral distribution. Here, the detector is operated so that the probability of observing an x-ray quantum in the detector for a given shot is about 0.1. The amplitude of response to this photon is a lower bound of x-ray energy, due to the preponderance of Compton escape events in the detector [8]. Figure 2 shows the response of the detector and the filter combinations used to evaluate the data. The detector response was checked with calibrated γ-ray sources (at 122, 384, 511, 835, and 1274 keV) in the geometry of the experiment. The filter transmissions were determined from tabulated data [9]. Not shown, but included in the calibration, are the 3.15-mm acrylic window of the vacuum chamber and the 0.5-mm aluminum encasement of the NaI crystal. The absorber foils were mounted just upstream of the first collimator, so that filter fluorescence and scattering into the detector is negligible.

Figure 3 shows the average detected x-ray yield from a tantalum target for various attenuators, plotted as a function of incident laser energy. The units of μJ/sr are derived by assuming the x rays originate from a point source, and dividing the energy deposited in the detector by the solid angle formed by the detector aperture. The data points represent the average for all laser shots within a 2-mJ range (typically 50 shots). However, considerable shot-to-shot fluctuation is observed in the x-ray yield.

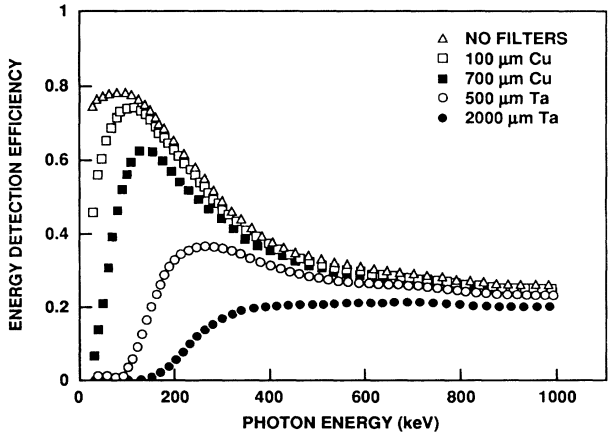

FIG. 2. Energy detection efficiency for the 25.4-mm NaI crystal and various metal filters as a function of photon energy. The NaI detector efficiency was checked with calibrated γ-ray standards; the metal filter transmissions were calculated from tabulated data [9].

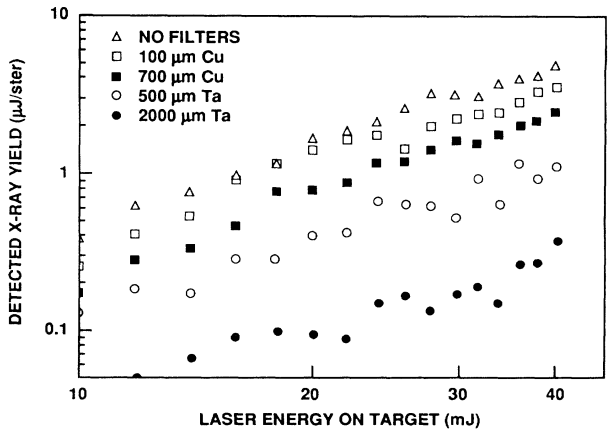

FIG. 3. Average detected x-ray yield as a function of incident laser energy and metal filter for a 1-mm-thick tantalum target, plotted on a log-log scale.

Some of the fluctuation may be caused by the target surface quality or vibrations in the target manipulator. The single-shot x-ray yield points are approximately normally distributed about the average. For the case of 40 mJ on the target and no filters, the average detected x-ray yield is 4.5 μJ/sr, and the rms fluctuation is 1.8 μJ/sr. Note that 25% of the detected x-ray energy passes through the 500-μm Ta filter, which has a $1/e$ transmission energy of about 175 keV. We assume that the x-ray radiation is isotropic when we convert this measured μJ/sr value to an overall yield.

Figure 4 shows the pulse-height spectrum for 40 mJ of incident laser energy onto a tantalum target. The detector aperture collects 1.2 μsr, and a 19-mm lead filter is used to further attenuate the x-ray beam. This thickness of lead extinguishes all photons less than about 350 keV. This configuration allows a detected event every 10 laser shots. Time coincidence with the laser pulse is used to eliminate background events. The second, diagnostic NaI detector data are used to insure that the yield fluctuation does not produce accidental counts, that is, all displayed counts were recorded from laser shots having similar x-ray yields. Figure 4 reduces to an average 0.02 μJ/sr per shot of x rays transmitted by 19 mm of lead, or 0.5% of the total x-ray yield.

Both methods of spectral determination are indirect, and any conclusions must be obtained by deconvolving the detector-filter response from the displayed data. We find that an assumed $1/E$ x-ray spectral distribution fits the data obtained with the less-opaque filters. The calculated detected energy transmitted through the 500-μm Al, 100-μm Cu, 700-μm Cu, and 500-μm Ta filters matches the measured value within 15%, assuming a $1/E$ x-ray energy spectrum between 20 and 300 keV (distribution parameter -1). A distribution parameter of either $-\frac{1}{2}$ or $-\frac{3}{2}$ causes this match to err by nearly 100%. The data deviate from this distribution beginning with the 2-mm tantalum filter, indicating that the distribution falls faster than $1/E$ at higher energies. The pulse-height analysis data show that while the spectrum is dropping rapidly at high energy, it does not drop exponentially. The apparent peak at 0.5 MeV is due to the turn-on of the lead filter transmission. Counts below this turn-on are Compton escape counts, which in general causes the deposited energy spectrum to be more heavily weighted at the low energy end than the actual photon spectrum. Within the bounds of our data, we do not observe a spectral cutoff or a characteristic temperature.

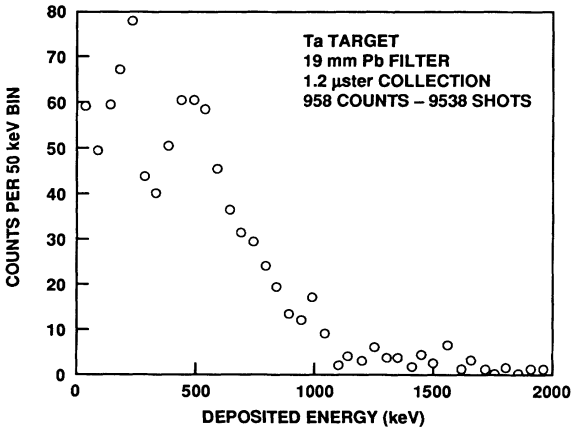

FIG. 4. Pulse-height spectrum for a tantalum target and 40 mJ of incident laser energy. The combination of a small solid angle of collection and a 19-mm lead filter limit the count rate to 0.1 event per shot. At these photon energies, the detector most likely registers a Compton escape peak, rather than the full photon energy.

We find that the x-ray spectral distribution is not a strong function of incident laser energy, within our dynamic range (10 to 40 mJ). However, the detected x-ray yield increases as the $\frac{3}{2}$ power of the incident laser energy. We have also used materials other than tantalum for the target, such as aluminum, silica, and 12-μm Ag-coated silica. The relative x-ray yields (above 20 keV) are 0.19, 0.16, and 0.36 with respect to the tantalum yield. Hence, the x-ray yield is proportional to the atomic number of the target. The silver target produces fewer x rays than that predicted by its atomic number, suggesting that some of the x rays originate from depths greater than 12 μm, where the target material becomes silica. The spectral distribution of the x rays does not appear to depend on the atomic number; only the yield shows any significant variation.

We have demonstrated an efficient source of hard x rays. The significant new features of this source are the potential short time duration and small source size. The radiation probably arises from hot electrons emitting bremsstrahlung radiation while propagating in the solid density target. The efficiency of a traditional electron-beam-driven x-ray tube is roughly $10^{-9}ZV$, where Z is the atomic number of the target and V is the cathode-anode voltage. We note that our efficiency appears to follow this relation, where V represents the square root of the laser beam intensity. To achieve comparable generation, a 1-MeV electron gun would require a subpicosecond current pulse of around 10 kA and a repetition rate of 5 Hz. To predict the source size and pulse duration, consider that a 1-MeV electron traveling in solid tantalum has a stopping range of about 250 μm, much larger than the laser-plasma interaction range (~ 10 μm). If there are no other pulse lengthening processes, this implies an x-ray pulse of order 500 fsec, due to the transit times of the electrons and photons. These numbers suggest that this laser-driven source substantially extends the parameter range of pulsed x-ray generation.

The authors would like to acknowledge discussions with S. Benerofe. This research was supported by the U.S. Air Force Office of Scientific Research, the U.S. Army Research Office, and the Strategic Defense Initia-

tive Organization, and by the Department of Energy, Office of Basic Energy Science, Division of Materials Sciences.

---

[a]Present addresses: Stanford Synchrotron Radiation Laboratory, Stanford University, Stanford, CA 94305, and Department of Physics, University of California, Santa Cruz, Santa Cruz, CA 95064.

[1] J. D. Kmetec, J. J. Macklin, and J. F. Young, Opt. Lett. **16**, 1001 (1991).

[2] M. M. Murnane, H. C. Kapteyn, M. D. Rosen, and R. W. Falcone, Science **251**, 531 (1991).

[3] A. Zigler, P. G. Burkhalter, D. J. Nagel, K. Boyer, T. S. Luk, A. McPherson, J. C. Solem, and C. K. Rhodes, Appl. Phys. Lett. **59**, 777 (1991).

[4] J. A. Cobble, G. A. Kyrala, A. A. Hauer, A. J. Taylor, C. C. Gomez, N. D. Delamater, and G. T. Schappert, Phys. Rev. A **39**, 454 (1989).

[5] H. M. Milchberg, I. Lyubomirsky, and C. G. Durfee, III, Phys. Rev. Lett. **67**, 2654 (1991).

[6] S. E. Harris and J. D. Kmetec, Phys. Rev. Lett. **61**, 62 (1988).

[7] W. L. Kruer, *The Physics of Laser Plasma Interactions* (Addison-Wesley, New York, 1988).

[8] G. F. Knoll, *Radiation Detection and Measurement* (Wiley, New York, 1989), 2nd ed.

[9] W. J. Veigele, At. Data **5**, 51 (1973).